

Measurement of the generalized spin polarizabilities of the neutron in the low Q^2 region

Vincent Sulkosky,^{1,2,3} Chao Peng,^{4,5} Jian-ping Chen,² Alexandre Deur*,^{3,2} Sergey Abrahamyan,⁶ Konrad A. Aniol,⁷ David S. Armstrong,¹ Todd Averett,¹ Stephanie L. Bailey,¹ Arie Beck,⁸ Pierre Bertin,⁹ Florentin Butaru,¹⁰ Werner Boeglin,¹¹ Alexandre Camsonne,⁹ Gordon D. Cates,³ Chia-Cheh Chang,¹² Seonho Choi,¹⁰ Eugene Chudakov,² Luminita Coman,¹¹ Juan C. Cornejo,⁷ Brandon Craver,³ Francesco Cusanno,¹³ Raffaele De Leo,¹⁴ Cornelis W. de Jager^{†,2} Joseph D. Denton,¹⁵ Seema Dhamija,¹⁶ Robert Feuerbach,² John M. Finn^{†,1} Salvatore Frullani^{†,13,17} Kirsten Fuoti,¹ Haiyan Gao,¹⁸ Franco Garibaldi,^{13,17} Olivier Gayou,⁸ Ronald Gilman,^{2,19} Alexander Glamazdin,²⁰ Charles Glashausser,¹⁹ Javier Gomez,² Jens-Ole Hansen,² David Hayes,²¹ F. William Hersman,²² Douglas W. Higinbotham,² Timothy Holmstrom,^{1,15} Thomas B. Humensky,³ Charles E. Hyde,²¹ Hassan Ibrahim,^{21,23} Mauro Iodice,¹³ Xiandong Jiang,¹⁹ Lisa J. Kaufman,²⁴ Aidan Kelleher,¹ Kathryn E. Keister,¹ Wooyoung Kim,²⁵ Ameya Kolarkar,¹⁶ Norm Kolb,²⁶ Wolfgang Korsch,¹⁶ Kevin Kramer,^{1,4} Gerfried Kumbartzki,¹⁹ Luigi Lagamba,¹⁴ Vivien Lainé,^{2,9} Geraud Laveissiere,⁹ John J. Leroose,² David Lhuillier,²⁷ Richard Lindgren,³ Nilanga Liyanage,^{3,2} Hai-Jiang Lu,²⁸ Bin Ma,⁸ Demetrius J. Margaziotis,⁷ Peter Markowitz,¹¹ Kathleen R. McCormick,¹⁹ Mehdi Meziane,⁴ Zein-Eddine Meziani,¹⁰ Robert Michaels,² Bryan Moffit,¹ Peter Monaghan,⁸ Sirish Nanda,² Jennifer Niedziela,²⁴ Mikhail Niskin,¹¹ Ronald Pandolfi,²⁹ Kent D. Paschke,²⁴ Milan Potokar^{†,30} Andrew Puckett,³ Vina A. Punjabi,³¹ Yi Qiang,⁸ Ronald D. Ransome,¹⁹ Bodo Reitz,² Rikki Roché,³² Arun Saha^{†,2} Alexander Shabetai,¹⁹ Simon Širca,³³ Jaideep T. Singh,³ Karl Slifer,¹⁰ Ryan Snyder,³ Patricia Solvignon^{†,10} Ronald Stringer,⁴ Ramesh

* Corresponding author; E-mail: deurpam@jlab.org.

† Deceased.

Subedi[†],³⁴ William A. Tobias,³ Ngyen Ton,³ Paul E. Ulmer,²¹ Guido Maria Urciuoli,¹³ Antonin Vacheret,²⁷ Eric Voutier,³⁵ Kebin Wang,³ Lu Wan,⁸ Bogdan Wojtsekhowski,³⁶ Seungtae Woo,²⁵ Huan Yao,¹⁰ Jing Yuan,¹⁹ Xiaohui Zhan,⁸ Xiaochao Zheng,^{5,3} and Lingyan Zhu⁸
 (Jefferson Lab E97-110 Collaboration)

¹*William & Mary, Williamsburg, Virginia 23187-8795, USA*

²*Thomas Jefferson National Accelerator Facility, Newport News, Virginia 23606, USA*

³*University of Virginia, Charlottesville, Virginia 22904, USA*

⁴*Duke University, Durham, North Carolina 27708, USA*

⁵*Argonne National Laboratory, Lemont, Illinois 60439, USA*

⁶*Yerevan Physics Institute, Yerevan 375036, Armenia*

⁷*California State University, Los Angeles, Los Angeles, California 90032, USA*

⁸*Massachusetts Institute of Technology, Cambridge, Massachusetts 02139, USA*

⁹*LPC Clermont-Ferrand, Université Blaise Pascal, CNRS/IN2P3, F-63177 Aubière, France*

¹⁰*Temple University, Philadelphia, Pennsylvania 19122, USA*

¹¹*Florida International University, Miami, Florida 33199, USA*

¹²*University of Maryland, College Park, Maryland 20742, USA*

¹³*Istituto Nazionale di Fisica Nucleare, Sezione di Roma, I-00185 Rome, Italy*

¹⁴*Istituto Nazionale di Fisica Nucleare, Sezione di Bari and University of Bari, I-70126 Bari, Italy*

¹⁵*Longwood University, Farmville, VA 23909, USA*

¹⁶*University of Kentucky, Lexington, Kentucky 40506, USA*

¹⁷*Istituto Superiore di Sanità, I-00161 Rome, Italy*

¹⁸*Duke University and Triangle Universities Nuclear Laboratory, Durham, NC, USA*

¹⁹*Rutgers, The State University of New Jersey, Piscataway, New Jersey 08855, USA*

²⁰*Kharkov Institute of Physics and Technology, Kharkov 310108, Ukraine*

²¹*Old Dominion University, Norfolk, Virginia 23529, USA*

²²*University of New Hampshire, Durham, New Hampshire 03824, USA*

²³*Cairo University, Cairo, Giza 12613, Egypt*

²⁴*University of Massachusetts-Amherst, Amherst, Massachusetts 01003, USA*

²⁵*Kyungpook National University, Taegu City, South Korea*

²⁶*University of Saskatchewan, Saskatoon, SK S7N 5E2, Canada*

²⁷*DAPNIA/SPhN, CEA Saclay, F-91191 Gif-sur-Yvette, France*

²⁸*Department of Modern Physics, University of Science and Technology of China, Hefei 230026, China*

²⁹*Randolph-Macon College, Ashland, Virginia 23005, USA*

³⁰*Institut Jozef Stefan, University of Ljubljana, Ljubljana, Slovenia*

³¹*Norfolk State University, Norfolk, Virginia 23504, USA*

³²*Florida State University, Tallahassee, Florida 32306, USA*

³³*Faculty of Mathematics and Physics, University of Ljubljana, Slovenia*

³⁴*Kent State University, Kent, Ohio 44242, USA*

³⁵*LPSC, Université Joseph Fourier, CNRS/IN2P3, INPG, F-38026 Grenoble, France*

³⁶*Thomas Jefferson National Accelerator Facility, Newport News, Virginia 23606, USA*

(Dated: February 25, 2022)

Understanding the nucleon spin structure in the regime where the strong interaction becomes truly strong poses a challenge to both experiment and theory. At energy scales below the nucleon mass of about 1 GeV, the intense interaction among the quarks and gluons inside the nucleon makes them highly correlated. Their coherent behaviour causes the emergence of effective degrees of freedom, requiring the application of non-perturbative techniques, such as chiral effective field theory [1]. Here, we present measurements of the neutron's generalized spin-polarizabilities that quantify the neutron's spin precession under electromagnetic fields at very low energy-momentum transfer squared down to 0.035 GeV². In this regime, chiral effective field theory calculations [2–4] are expected to be applicable. Our data, however, show a strong discrepancy with these predictions, presenting a challenge to the current description of the neutron's spin properties.

The nucleon is the basic building block of nature, accounting for about 99% of the universe's

visible mass. Understanding its properties, e.g., mass and spin, is thus crucial. Those are mainly determined by the Strong Interaction, which is described by Quantum Chromodynamics (QCD) with quarks and gluons as the fundamental degrees of freedom. The nucleon structure is satisfactorily understood at high Q^2 (short space-time scales, see Fig. 1 for the definition of kinematic variables), since there QCD is calculable using perturbation methods (perturbative QCD) and tested by numerous experimental measurements. At lower Q^2 , the strong coupling α_s becomes too large for perturbative QCD to be applicable [5]. Yet, calculations are critically needed since the Strong Interaction's chiral symmetry breaks in this region. Chiral symmetry and its breaking is one of the most important properties of the Strong Interaction and is believed to lead to the emergence of the nucleon's global properties. To understand how the underlying structure leads to the emergence of these global properties, non-perturbative methods must be used. A method using the fundamental quark and gluon degrees of freedom is lattice QCD. However, calculations from this method are often intractable for spin observables at low Q^2 [6]. Another solution is to employ effective theories. Chiral effective field theory (χ EFT) capitalizes on QCD's approximate chiral symmetry and uses the emergent hadronic degrees of freedom. Therein lies χ EFT's strengths and challenges: while the nucleon and the pion are used for first-order calculations, this is often insufficient to describe the data, and heavier hadrons, such as the nucleon's first excited state $\Delta(1232)$, become needed. This complicates χ EFT calculations, and theorists are still seeking the best way to include the $\Delta(1232)$ in their calculations. It is therefore crucial to perform precision measurements at low enough Q^2 to test χ EFT calculations. Spin observables, among them the generalized spin-polarizabilities that are reported here, provide an extensive set of tests to benchmark χ EFT calculations [6].

Polarizabilities describe how the components of an object collectively react to external electromagnetic fields. In particular, spin-polarizabilities quantify the object's spin precession under an electromagnetic field. The spin-polarizabilities, initially defined with real photons, can

be generalized to virtual photons such as those used to probe the neutron in our experiment. Accordingly, generalized spin-polarizabilities are extracted by scattering polarized electrons off polarized nucleons and measuring how the cross-section changes when the relative orientation between the electron and nucleon spins is varied (see Fig. 1). The energy-momentum

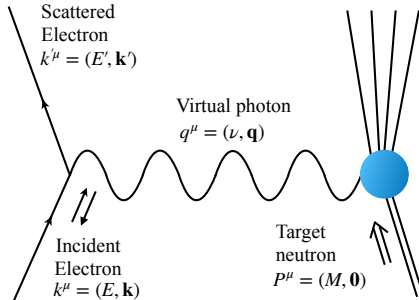


FIG. 1: Electron scattering off a neutron by the one-photon exchange process. The 4-momenta of the incident and the scattered electrons are $k^\mu = (E, \mathbf{k})$ and $k'^\mu = (E', \mathbf{k}')$, respectively, and that of the photon is $q^\mu = (\nu, \mathbf{q})$. The neutron, at rest in the laboratory frame, has a 4-momentum $P^\mu = (M, \mathbf{0})$. The arrows $\uparrow\downarrow$ represent the spin direction of the incident electron and $\uparrow\uparrow$ that of the neutron. The generalized spin-polarizabilities of the neutron can be measured when both the incident electron and the neutron are polarized.

transferred between the electron and neutron is (ν, \mathbf{q}) , with $Q^2 = \mathbf{q}^2 - \nu^2$ characterizing the space-time scale at which we probe the neutron. While real photons ($Q^2 = 0$) only have transverse polarizations, mediating virtual photons ($Q^2 \neq 0$) are transversely (T) or longitudinally (L) polarized. Thus, two contributions to the spin-polarizability arise: one from the transverse-transverse (TT) interference called the forward spin-polarizability $\gamma_0(Q^2)$, and the other from the longitudinal-transverse (LT) interference, called the Longitudinal-Transverse interference polarizability $\delta_{LT}(Q^2)$, which is available only with virtual photons. The additional longitudinal polarization direction and the ensuing interference term offer extra latitude to test theories describing the Strong Interaction.

The theoretical basis to measure $\delta_{\text{LT}}(Q^2)$ originates from a work of Gell-Mann, Goldberger and Thirring [7, 8]. This work led to relations between the cross-sections measured in polarized electron-nucleon scattering (Fig. 1) and the spin-polarizabilities:

$$\gamma_0(Q^2) = \frac{1}{2\pi^2} \int_{\nu_0}^{\infty} \frac{\kappa_\gamma}{\nu^2} \frac{\sigma_{\text{TT}}(\nu, Q^2)}{\nu^2} d\nu, \quad (1)$$

$$\delta_{\text{LT}}(Q^2) = \left(\frac{1}{2\pi^2} \right) \int_{\nu_0}^{\infty} \frac{\kappa_\gamma}{\nu Q} \frac{\sigma_{\text{LT}}(\nu, Q^2)}{\nu^2} d\nu, \quad (2)$$

where $\kappa_\gamma = \nu - Q^2/2M$ [9] is the photon flux factor, ν_0 the photoproduction threshold, and σ_{TT} and σ_{LT} are respectively the TT and LT interference cross-sections. They are obtained from [6, 10]:

$$\sigma_{\text{TT}}(\nu, Q^2) = \frac{\pi^2 E Q^2 (1 - \epsilon)}{\alpha \kappa_\gamma E' (1 - \epsilon E'/E) (1 + \eta \zeta)} \left(\sqrt{\frac{2\epsilon}{1 + \epsilon}} \Delta\sigma_{\parallel}(\nu, Q^2) - \eta \Delta\sigma_{\perp}(\nu, Q^2) \right), \quad (3)$$

$$\sigma_{\text{LT}}(\nu, Q^2) = \frac{\pi^2 E Q^2 (1 - \epsilon)}{\alpha \kappa_\gamma E' (1 - \epsilon E'/E) (1 + \eta \zeta)} \left(\sqrt{\frac{2\epsilon}{1 + \epsilon}} \zeta \Delta\sigma_{\parallel}(\nu, Q^2) + \Delta\sigma_{\perp}(\nu, Q^2) \right), \quad (4)$$

where $\Delta\sigma_{\parallel}$ ($\Delta\sigma_{\perp}$) is the difference between the cross sections when the beam and target spin directions are parallel and antiparallel (perpendicular), α is the electromagnetic coupling constant, $\epsilon = 1/[1 + 2(1 + Q^2/4M^2x^2) \tan^2(\theta/2)]$ with $x = Q^2/2m\nu$ the Bjorken scaling variable and θ the electron scattering angle in the laboratory frame, $\eta = \epsilon Q/(E - E'\epsilon)$ and $\zeta = \eta(1 + \epsilon)/2\epsilon$. The σ_{TT} and σ_{LT} , shown in Figs. 2 and 3, were integrated according to Eqs. (1) and (2) to obtain $\gamma_0(Q^2)$ and $\delta_{\text{LT}}(Q^2)$. The unmeasured part of the integrals at large ν is often negligible due to the ν -weighting.

An outstanding feature of $\delta_{\text{LT}}(Q^2)$ at low Q^2 is that the $\Delta(1232)$ is not expected to appreciably contribute to the LT-interference cross section, since exciting the $\Delta(1232)$ overwhelmingly involves transverse photons. This should alleviate the difficulty of including the $\Delta(1232)$ in χ EFT calculations, making them more robust. However, the first measurement of $\delta_{\text{LT}}(Q^2)$ from

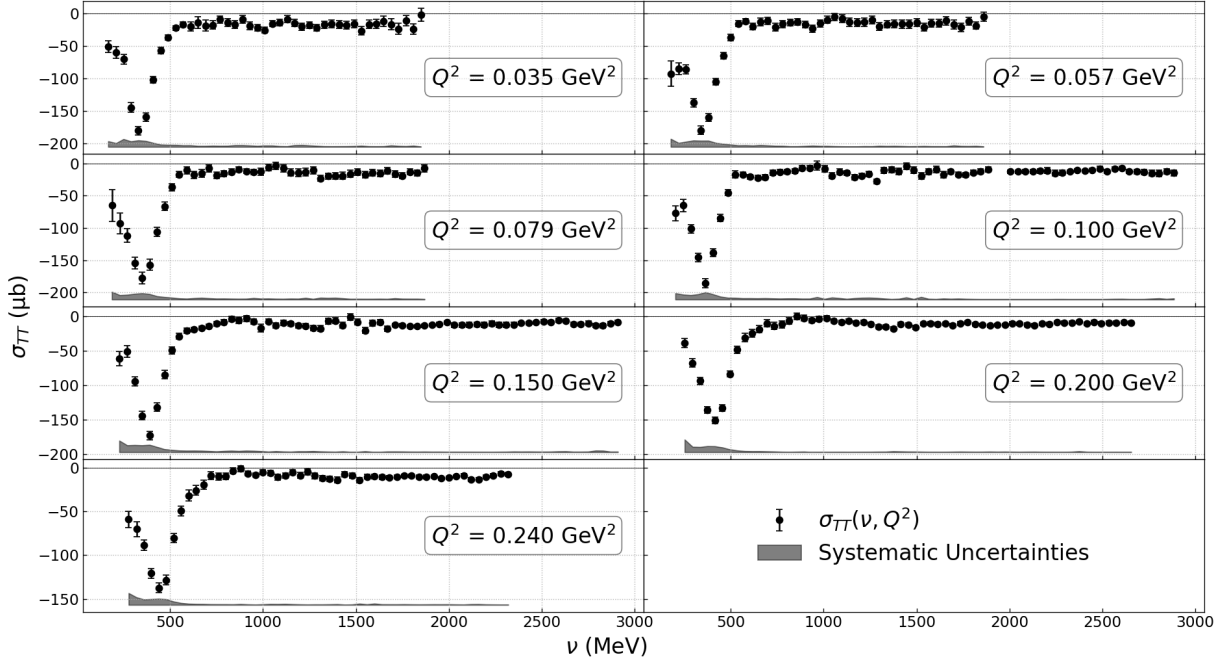


FIG. 2: The transverse-transverse cross-section $\sigma_{TT}(\nu, Q^2)$ for ${}^3\text{He}$. The data are displayed at the Q^2 values at which they are integrated to form γ_0 (Eq. 1). The error bars, sometimes too small to be visible, represent the statistical uncertainties. The systematic uncertainty is indicated by the band at the bottom of each panel. The nuclear corrections providing the neutron information from the ${}^3\text{He}$ data are applied after the integration. The prominent negative peak at small- ν is the $\Delta(1232)$ contribution.

JLab experiment E94-010 [11] done at $Q^2 \geq 0.1 \text{ GeV}^2$ strongly disagreed with χ EFT calculations [12, 13]. This surprising result, known as the “ δ_{LT} puzzle” [10], triggered improved χ EFT calculations [14] which now explicitly include the $\Delta(1232)$ [2–4], and measurements of δ_{LT} at lower Q^2 where χ EFT can be best tested. New data of δ_{LT} on the neutron at very low Q^2 are presented next, which were taken during experiment JLab E97-110.

Eq. (2) allows measuring $\delta_{LT}^n(Q^2)$ (the superscript n indicates neutron quantities) by scattering polarized electrons off polarized neutrons in ${}^3\text{He}$ nuclei. The data were acquired in Hall A [15] of Jefferson Lab (JLab) during experiment E97-110 [16]. The probing virtual photons were produced by a longitudinally polarized electron beam during its scattering off a polarized

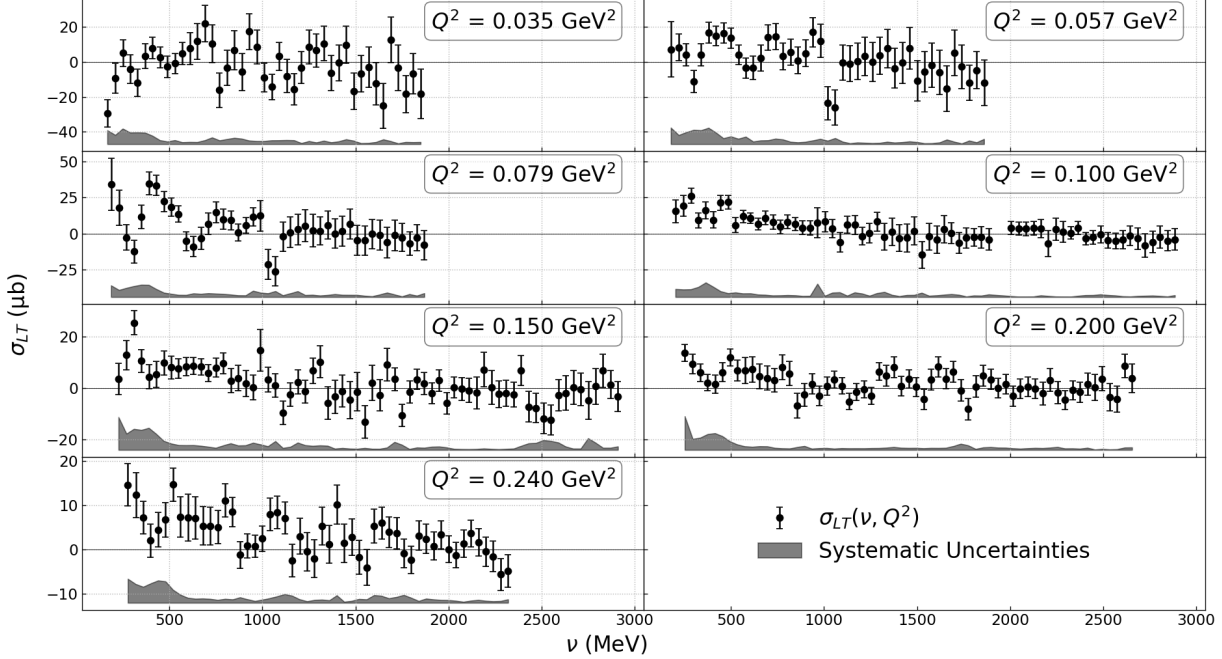


FIG. 3: The longitudinal-transverse interference cross-section $\sigma_{LT}(\nu, Q^2)$ for ${}^3\text{He}$. The data are displayed at the Q^2 values at which they are integrated into $\delta_{LT}(Q^2)$ (Eq. 2) or $I_{LT}(Q^2)$ (Eq. 5). The error bars represent the statistical uncertainties. The systematic uncertainty is indicated by the band at the bottom of each panel. The nuclear corrections [18] necessary to obtain the neutron information from the ${}^3\text{He}$ data are applied after the integration. The prominent $\Delta(1232)$ contribution seen for $\sigma_{TT}(\nu, Q^2)$ in Fig. 2 is not present here, in agreement with the expectation that the role of $\Delta(1232)$ is suppressed in LT-interference quantities.

${}^3\text{He}$ target [15]. The beam polarization, flipped pseudo-randomly at 30 Hz and monitored by Møller and Compton polarimeters, was $(75.0 \pm 2.3)\%$. The beam energies ranged from 1.1 to 4.4 GeV, and the beam current was typically a few μA . Since free neutrons are unstable, we used ${}^3\text{He}$ nuclei as an effective polarized neutron target. To first-order, polarized ${}^3\text{He}$ nuclei can be treated as effective polarized neutrons together with unpolarized protons because the ${}^3\text{He}$'s nucleons (two protons and one neutron) are mostly in an S -state, and so the Pauli exclusion principle dictates that in the S -state the proton spins point oppositely, yielding no net

contribution to the ${}^3\text{He}$ spin. The gaseous (≈ 12 atm) ${}^3\text{He}$ was contained in a 40 cm-long glass cylinder and polarized by spin-exchange optical pumping of Rubidium atoms. Helmholtz coils provided a longitudinal or transverse 2.5 mT field used to maintain the polarization, to orient it longitudinally or transversely (in-plane) to the beam direction, and to aid in performing polarimetry. The average target polarization in-beam was $(39.0 \pm 1.6)\%$. The scattered electrons from the reaction ${}^3\vec{\text{He}}(\vec{e}, e')$ were detected by a High Resolution Spectrometer (HRS) [15] supplemented by a dipole magnet [17] allowing us to detect electrons scattered at angles down to 6° . Behind the HRS, drift chambers provided particle tracking, scintillator planes enabled the data acquisition trigger, and a gas Cherenkov counter and electromagnetic calorimeters ensured the identification of the particle type.

The measured σ_{TT} (σ_{LT}) on ${}^3\text{He}$ is shown in Fig. 2 (Fig. 3). Its values with their uncertainties are available in the Supplementary Data Files. While polarized ${}^3\text{He}$ nuclei are effectively polarized neutrons to good approximation, nuclear corrections are needed to obtain genuine neutron information. The prescription of Ref. [18] was used for the correction. The effect of the nuclear correction, which can be obtained from Tables I-III in the Supplementary Data Files, is relatively small. In particular it does not appreciably affect the Q^2 trend seen for the uncorrected ${}^3\text{He}$ integrals. The relative uncertainty on this correction is estimated to be 6 to 14% relative to the correction, the higher uncertainties corresponding to our lowest Q^2 values. The quasi-elastic contamination was corrected following the procedure described in [16]. The correction is small for δ_{LT}^n , but important for γ_0^n and was estimated using [19]. No calculation uncertainty is provided in [19] and using another quasi-elastic calculation [20] may shift the lowest- Q^2 γ_0^n data points by as much as our total systematic uncertainty. The other main systematic uncertainties come from the absolute cross-sections (3.5 to 4.5%), target and beam polarizations (3 to 5% and 3.5%, respectively), and radiative corrections (3 to 7%).

Our $\delta_{\text{LT}}^n(Q^2)$ data are shown in the left panel of Fig. 4. They agree with earlier data from

E94-010 at larger Q^2 [11] while reaching much lower Q^2 where the χ EFT is expected to work well. The measurement can be compared to χ EFT calculations [2, 4, 12, 13] and a model parameterization of the world photo- and electro-production data called MAID [21]. Earlier χ EFT

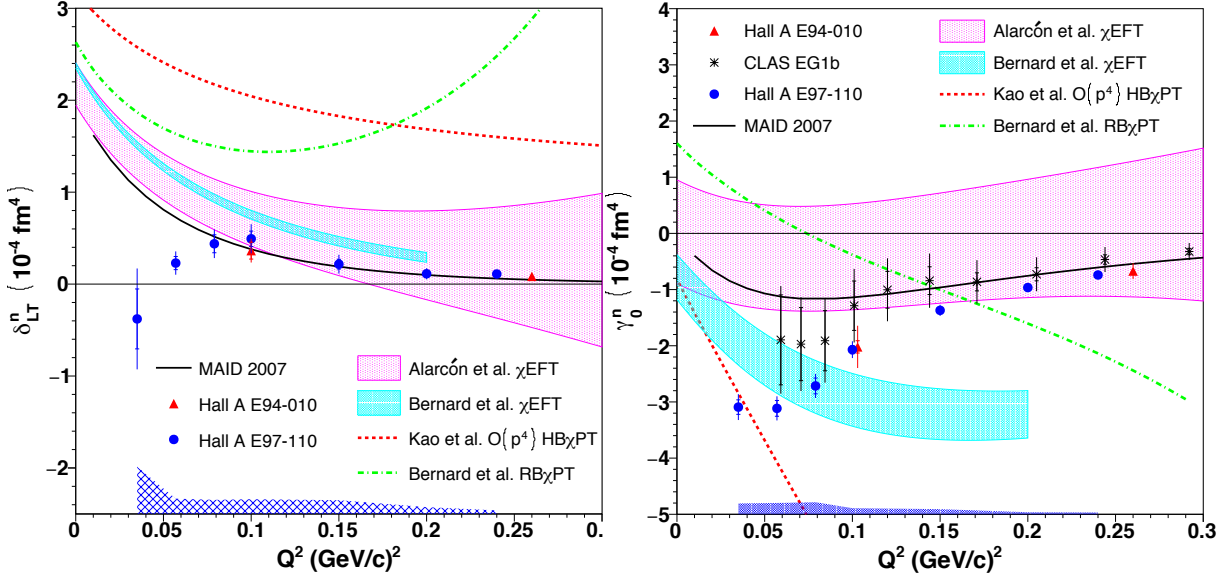


FIG. 4: The generalized spin polarizabilities $\delta_{LT}^n(Q^2)$ and $\gamma_0^n(Q^2)$. Left: The generalized spin-polarizability $\delta_{LT}^n(Q^2)$. The circles represent the results from experiment E97-110. They can be compared to earlier E94-010 data [11] (triangles) and theoretical calculations: the older χ EFT calculations [12] (dot-dashed line) and [13] (dashed line) in which the Δ resonance contribution is not included or included phenomenologically, the state-of-the-art calculations [2] (cyan band) and [4] (magenta band) that include the Δ , as well as the MAID model [21] (black curve) which is a fit to world resonance data. For the E97-110 data, the inner error bars, sometimes too small to be visible, represent the statistical uncertainties. The outer error bars show the statistical and uncorrelated systematic uncertainties. The correlated systematic uncertainty is indicated by the band at the bottom. For the other experimental data, the error bars show the statistical and systematic uncertainties added in quadrature. Right: The generalized forward spin-polarizability $\gamma_0^n(Q^2)$, using the same symbols as in the left panel. The asterisks represent the CLAS data [22].

calculations [12, 13] used different approaches (Heavy Baryon and Relativistic Baryon chiral

perturbation theory: HB χ PT and RB χ PT, respectively), and furthermore either neglected the $\Delta(1232)$ degrees of freedom, or included it approximately. Newer calculations [2–4], which are all fully relativistic, account for the $\Delta(1232)$ explicitly by using a perturbative expansion, but they differ in their choice of expansion parameter. Despite this theoretical improvement and the small- Q^2 reach that places our data well in the validity domain of χ EFT, our $\delta_{\text{LT}}^n(Q^2)$ starkly disagrees with the predictions. This is even more surprising because the latest χ EFT calculations of δ_{LT}^n agree with each other, suggesting that calculations for this particular observable should be under control. However, our data reveal an opposite trend with Q^2 to that of all the χ EFT calculations.

This startling discrepancy demanded further scrutinization of our data. They are compatible with the E94-010 data where they overlap. This is also true for $\gamma_0^n(Q^2)$, which we measured concurrently and show in the right panel of Fig. 4. The measured $\gamma_0^n(Q^2)$ also agrees with data from CLAS experiment EG1 [22], which used a target and detectors that are very different from E97-110 and E94-010. Our $\gamma_0^n(Q^2)$ data generally disagree with χ EFT calculations. Since $\gamma_0(Q^2)$ does not benefit from the suppression of the $\Delta(1232)$ contribution, and since $\gamma_0^n(Q^2)$ predictions do not reach a consensus, this disagreement is not entirely surprising, in contrast to the unexpected $\delta_{\text{LT}}^n(Q^2)$ disagreement. Interestingly, we can also study with our data the Schwinger relation [23], which has a similar definition but without ν^{-2} weighting in its integrand:

$$I_{\text{LT}}(Q^2) \equiv \left(\frac{M^2}{\alpha\pi^2} \right) \int_{\nu_0}^{\infty} \left[\kappa_{\gamma} \frac{\sigma_{\text{LT}}(\nu, Q^2)}{Q\nu} \right]_{Q=0} d\nu. \quad (5)$$

Schwinger predicted that $I_{\text{LT}}(Q^2) \xrightarrow{Q^2 \rightarrow 0} \kappa e_t$, with κ the anomalous magnetic moment of the target particle and e_t its electric charge. This prediction is general, e.g. it does not use χ EFT. $I_{\text{LT}}(Q^2)$ having no $1/\nu^2$ -weighting, the large ν contribution to the integral is not negligible. Since this contribution to the integral cannot be measured, a parameterization based on the model described in [24] completed by a Regge-based parameterization [25] for the largest ν part was

used to extrapolate it. Our measurement of $I_{\text{LT}}^n(Q^2)$ is shown in Fig. 5. Our measurement of $I_{\text{LT}}^n(Q^2)$ without the Regge-based parameterization [25] for the large- ν part (open symbols), which is suppressed in $\delta_{\text{LT}}(Q^2)$, displays a similar pattern as $\delta_{\text{LT}}^n(Q^2)$. The Gerasimov-Drell-Hearn (GDH) relation [28, 29] can be used to extrapolate our $I_{\text{LT}}^n(Q^2)$ to $Q^2 = 0$; and provided that the GDH relation is valid, which is widely expected and supported by dedicated experimental studies [30], our data satisfy Schwinger’s prediction that $I_{\text{LT}}^n(0) = 0$ [23]. Our trend contrasts with the MAID model and presumably the χ EFT calculations, since MAID tracks those (see Fig. 4). This suggests that the problem lies in the theoretical description of the neutron structure. The measured $I_{\text{LT}}(Q^2)$ displays a similar Q^2 -behavior as δ_{LT} , irrespective of the different ν -weighting. Other integrals without ν^{-2} weighting formed using our data and reported in [16] did not display the surprisingly strong disagreement with the predictions seen here. The values of γ_0^n , δ_{LT}^n and I_{LT}^n with their uncertainties are available in the Supplementary Data Files.

Our data indicate that both the TT and LT interferences of the electromagnetic field’s components induce a clear spin precession of the neutron. While it was predicted by all calculations and models that the LT term influence should intensify at small Q^2 , our data reveal the opposite trend. This notable disagreement is perplexing since our measurements were done well into the domain where χ EFT is expected to describe reliably the nucleon properties, especially the “gold-plated” δ_{LT} . Lattice QCD calculations of $\delta_{\text{LT}}(Q^2)$ are possible [31], but not yet available. Our data motivate such calculations since the measured generalized spin-polarizabilities underline a current lack of reliable quantitative descriptions of the Strong Interaction at the nucleon-size scale.

Data availability All experimental data that support the findings of this study are provided in the Supplementary Data Files or are available from J.P. Chen (jpchen@jlab.org), A. Deur (deurpam@jlab.org), C. Peng (cpeng@jlab.org) or V. Sulkosky (vasulk@jlab.org) upon request.

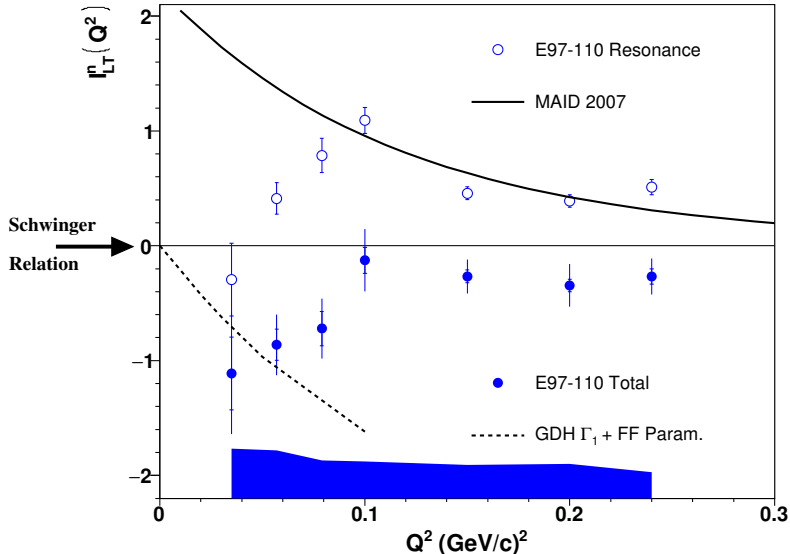


FIG. 5: The Schwinger integral $I_{LT}^n(Q^2)$. The open symbols are our results without the large ν part of I_{LT} . The filled blue circles are our results for the full I_{LT} , using an estimate for the large ν contribution. The inner error bars represent the statistical uncertainties. The outer error bars show the combined statistical and uncorrelated systematic uncertainties. The correlated systematic uncertainty is indicated by the band. The Schwinger relation [23] for the neutron predicts $I_{LT}^n(0) = 0$ at $Q^2 = 0$. The plain line shows the MAID model [21], which is a fit to world resonance data (to be compared to the open symbols). The dashed line uses the GDH (Γ_1) [28, 29] and Burkhardt-Cottingham [26] relations, together with an elastic form factor (FF) parameterization [27], to obtain $I_{LT}^n(Q^2)$ for $Q^2 \rightarrow 0$.

Code availability The computer codes that support the plots within this paper and the findings of this study are available from J.P. Chen (jpchen@jlab.org), A. Deur (deurpam@jlab.org), C. Peng (cpeng@jlab.org) or V. Sulkosky (vasulk@jlab.org) upon request.

Author contributions The members of the Jefferson Lab E97-110 Collaboration constructed and operated the experimental equipment used in this experiment. All authors contributed to the data collection, experiment design and commissioning, data processing, data analysis or Monte

Carlo simulations. The following authors especially contributed to the main data analysis: J.P Chen, A. Deur, C. Peng and V. Sulkosky.

Competing interests The authors declare no competing interests.

Acknowledgments

We acknowledge the outstanding support of the Jefferson Lab Hall A technical staff and the Physics and Accelerator Divisions that made this work possible. We thank A. Deltuva, J. Golak, F. Hagelstein, H. Krebs, V. Lensky, U.-G. Meißner, V. Pascalutsa, G. Salmè, S. Scopetta and M. Vanderhaeghen for useful discussions and for sharing their calculations. We are grateful to V. Pascalutsa and M. Vanderhaeghen for suggesting to compare the data to the Schwinger relation. This material is based upon work supported by the U.S. Department of Energy, Office of Science, Office of Nuclear Physics under contract DE-AC05-06OR23177, and by the NSF under grant PHY-0099557.

- [1] Bernard, V., Kaiser, N. & Meissner, U. G. Chiral dynamics in nucleons and nuclei. [Int. J. Mod. Phys. E](#) **4**, 193-346 (1995).
- [2] Bernard, V., Epelbaum, E., Krebs, H. & Meissner, U. G. New insights into the spin structure of the nucleon. [Phys. Rev. D](#) **87**, 054032 (2013).
- [3] Lensky, V., Alarcón, J. M., & Pascalutsa, V. Moments of nucleon structure functions at next-to-leading order in baryon chiral perturbation theory. [Phys. Rev. C](#) **90**, 055202 (2014).
- [4] Alarcón, J. M., Hagelstein, F., Lensky, V. & Pascalutsa, V. Forward doubly-virtual Compton scattering off the nucleon in chiral perturbation theory: II. Spin-polarizabilities and moments of polarized structure functions. [Phys. Rev. D](#) **102**, 114026 (2020).

- [5] Deur, A., Brodsky, S. J. & de Teramond, G. F. The QCD Running Coupling. *Prog. Part. Nucl. Phys.* **90**, 1-74 (2016).
- [6] Deur, A., Brodsky, S. J. & de Teramond, G. F. The Spin Structure of the Nucleon. *Rep. Prog. Phys.*, **82**, 076201 (2019).
- [7] Gell-Mann, M., Goldberger, M. L. & Thirring, W. E. Use of causality conditions in quantum theory. *Phys. Rev.* **95**, 1612-1627 (1954).
- [8] Guichon, P. A. M., Liu, G. Q. & Thomas, A. W. Virtual Compton scattering and generalized polarizabilities of the proton. *Nucl. Phys. A* **591**, 606-638 (1995).
- [9] Hand, L. N. Experimental investigation of pion electroproduction. *Phys. Rev.* **129**, 1834-1846 (1963).
- [10] Chen, J. P. Moments of Spin Structure Functions: Sum Rules and Polarizabilities. *Int. J. Mod. Phys. E* **19**, 1893-1921 (2010).
- [11] Amarian M. et al. Measurement of the generalized forward spin-polarizabilities of the neutron. *Phys. Rev. Lett.* **93**, 152301 (2004).
- [12] Bernard, V., Hemmert, T. R. & Meissner, U. G. Spin structure of the nucleon at low-energies. *Phys. Rev. D* **67**, 076008 (2003).
- [13] Kao, C. W., Spitzenberg, T. & Vanderhaeghen, M. Burkhardt-Cottingham sum rule and forward spin-polarizabilities in heavy baryon chiral perturbation theory. *Phys. Rev. D* **67**, 016001 (2003).
- [14] Hagelstein, F. , Miskimen, R. & Pascalutsa, V. Nucleon Polarizabilities: from Compton Scattering to Hydrogen Atom. *Prog. Part. Nucl. Phys.* **88**, 29-97 (2016).
- [15] Alcorn J. et al. Basic Instrumentation for Hall A at JLab. *Nucl. Instrum. Meth. A* **522**, 294-346 (2004).
- [16] Sulkosky V. et al. Measurement of the ${}^3\text{He}$ Spin-Structure Functions and of Neutron (${}^3\text{He}$) Spin-Dependent Sum Rules at $0.035 \leq Q^2 \leq 0.24 \text{ GeV}^2$. *Phys. Lett. B* **805**, 135428 (2020).
- [17] Garibaldi F. et al. High-resolution hypernuclear spectroscopy at Jefferson Lab, Hall A. *Phys. Rev. C* **99**, 054309 (2019).
- [18] Ciofi degli Atti, C. & Scopetta, S. On the extraction of the neutron spin structure functions and the Gerasimov-Drell-Hearn integral from He-3 (e, e-prime) X data. *Phys. Lett. B* **404**, 223-229 (1997).

- [19] Deltuva, A., Fonseca, A. C. and Sauer, P. U. Momentum-space treatment of Coulomb interaction in three-nucleon reactions with two protons. *Phys. Rev. C* **71**, 054005 (2005)
- [20] Golak, J., Skibinski, R., Witala, H., Glockle, W., Nogga, A., and Kamada, H. Proton polarizations in polarized He-3 studied with the polarized-He-3 (polarized-e, e-prime p) d and polarized-He-3 (polarized-e, e-prime p) pn processes, *Phys. Rev. C* **72**, 054005 (2005)
- [21] Drechsel, D., Hanstein, O., Kamalov, S. S. & Tiator, L. A Unitary isobar model for pion photoproduction and electroproduction on the proton up to 1-GeV. *Nucl. Phys. A* **645**, 145-174 (1999).
- [22] Guler N. et al. Precise determination of the deuteron spin structure at low to moderate Q^2 with CLAS and extraction of the neutron contribution. *Phys. Rev. C* **92**, 055201 (2015).
- [23] Schwinger, J. S. Source Theory Viewpoints in Deep Inelastic Scattering. *Proc. Nat. Acad. Sci.* **72**, 1-5 (1975).
- [24] Adhikari K. P. et al. Measurement of the Q2-dependence of the deuteron spin structure function g_1 and its moments at low Q2 with CLAS. *Phys. Rev. Lett.* **120**, 062501 (2018).
- [25] Bass, S. D., Skurzok, M. & Moskal, P. Updating spin-dependent Regge intercepts. *Phys. Rev. C* **98**, 025209 (2018).
- [26] Burkhardt, H. & Cottingham, W. N. Sum rules for forward virtual Compton scattering. *Annals Phys.* **56**, 453-463 (1970).
- [27] Ye, Z., Arrington, J., Hill, R. J. & Lee, G. Proton and Neutron Electromagnetic Form Factors and Uncertainties. *Phys. Lett. B* **777**, 8-15 (2018).
- [28] Gerasimov, S. B. A Sum rule for magnetic moments and the damping of the nucleon magnetic moment in nuclei, Sov. J. Nucl. Phys. **2**, 430-433 (1966); Yad. Fiz. **2**, 598-602 (1965).
- [29] Drell, S. D. & Hearn, A. C. Exact Sum Rule for Nucleon Magnetic Moments, *Phys. Rev. Lett.* **16**, 908-911 (1966).
- [30] Helbing, K. The Gerasimov-Drell-Hearn Sum Rule. *Prog. Part. Nucl. Phys.* **57**, 405-469 (2006).
- [31] Chambers, A. J. et al. Nucleon Structure Functions from Operator Product Expansion on the Lattice. *Phys. Rev. Lett.* **118**, 242001 (2017).

Data tables

Q^2 [GeV 2]	ν_{max} (W_{max}) [GeV]	$\delta_{LT}^{^3He, res}(Q^2) \pm (\text{stat}) \pm (\text{syst})$ [10 $^{-4}$ fm 4]	$\delta_{LT}^{n, res}(Q^2) \pm (\text{stat}) \pm (\text{syst})$ [10 $^{-4}$ fm 4]	$\delta_{LT}^n(Q^2) \pm (\text{stat}) \pm (\text{syst})$ [10 $^{-4}$ fm 4]
0.035	1.690 (2.00)	$-0.356 \pm 0.280 \pm 0.583$	$-0.379 \pm 0.326 \pm 0.677$	$-0.383 \pm 0.326 \pm 0.677$
0.057	1.700 (2.00)	$0.174 \pm 0.061 \pm 0.169$	$0.229 \pm 0.071 \pm 0.197$	$0.225 \pm 0.071 \pm 0.197$
0.079	1.710 (2.00)	$0.360 \pm 0.084 \pm 0.168$	$0.439 \pm 0.098 \pm 0.195$	$0.435 \pm 0.098 \pm 0.195$
0.100	2.885 (2.49)	$0.410 \pm 0.072 \pm 0.180$	$0.493 \pm 0.083 \pm 0.209$	$0.491 \pm 0.083 \pm 0.209$
0.150	2.910 (2.48)	$0.178 \pm 0.045 \pm 0.149$	$0.216 \pm 0.053 \pm 0.173$	$0.215 \pm 0.053 \pm 0.173$
0.200	2.655 (2.38)	$0.091 \pm 0.024 \pm 0.078$	$0.112 \pm 0.028 \pm 0.091$	$0.111 \pm 0.028 \pm 0.091$
0.240	2.320 (2.23)	$0.090 \pm 0.017 \pm 0.041$	$0.110 \pm 0.020 \pm 0.043$	$0.108 \pm 0.020 \pm 0.043$

TABLE I: Data and kinematics for $\delta_{LT}(Q^2)$. From left to right: Four-momentum transfer squared; Maximum ν value experimentally covered (equivalent maximum invariant W ($W = (M^2 + 2M\nu - Q^2)^{1/2}$); $\delta_{LT}^{^3He, res}(Q^2)$ measured over the ν (W) range from pion threshold up to maximum ν (W) covered experimentally (mostly the nucleon resonance region) and before applying the nuclear corrections to extract the neutron information. (stat) denotes the statistical uncertainty and (syst) the systematic uncertainty; Extracted neutron $\delta_{LT}^{n, res}$ (resonance) after applying nuclear corrections to the previous column; Total $\delta_{LT}^n(Q^2)$. Comparing the two last columns shows that the unmeasured parts of $\delta_{LT}^n(Q^2)$, i.e, the contributions for $\nu > \nu_{max}$, are negligible.

Q^2 [GeV 2]	$\nu_{max} (W_{max})$ [GeV]	$\gamma_0^{^3He, res}(Q^2) \pm (\text{stat}) \pm (\text{syst})$ [10 $^{-4}$ fm 4]	$\gamma_0^{n, res}(Q^2) \pm (\text{stat}) \pm (\text{syst})$ [10 $^{-4}$ fm 4]	$\gamma_0^n(Q^2) \pm (\text{stat}) \pm (\text{syst})$ [10 $^{-4}$ fm 4]
0.035	1.690 (2.00)	$-2.590 \pm 0.111 \pm 0.225$	$-3.092 \pm 0.129 \pm 0.270$	$-3.094 \pm 0.129 \pm 0.270$
0.057	1.700 (2.00)	$-2.613 \pm 0.121 \pm 0.215$	$-3.115 \pm 0.141 \pm 0.259$	$-3.117 \pm 0.141 \pm 0.259$
0.079	1.710 (2.00)	$-2.274 \pm 0.121 \pm 0.226$	$-2.715 \pm 0.140 \pm 0.270$	$-2.717 \pm 0.140 \pm 0.270$
0.100	2.885 (2.49)	$-1.725 \pm 0.063 \pm 0.143$	$-2.070 \pm 0.074 \pm 0.170$	$-2.070 \pm 0.074 \pm 0.170$
0.150	2.910 (2.48)	$-1.135 \pm 0.044 \pm 0.105$	$-1.370 \pm 0.051 \pm 0.125$	$-1.370 \pm 0.051 \pm 0.125$
0.200	2.655 (2.38)	$-0.798 \pm 0.027 \pm 0.056$	$-0.964 \pm 0.032 \pm 0.065$	$-0.965 \pm 0.032 \pm 0.065$
0.240	2.320 (2.23)	$-0.612 \pm 0.022 \pm 0.043$	$-0.740 \pm 0.026 \pm 0.050$	$-0.742 \pm 0.026 \pm 0.050$

TABLE II: Data and kinematics for $\gamma_0(Q^2)$. From left to right: Four-momentum transfer squared; Maximum ν value experimentally covered (equivalent maximum invariant W ($W = (M^2 + 2M\nu - Q^2)^{1/2}$); $\gamma_0^{^3He, res}(Q^2)$ measured over the $\nu(W)$ range from pion threshold up to maximum $\nu(W)$ covered experimentally (mostly the nucleon resonance region) and before applying the nuclear corrections to extract the neutron information. (stat) denotes the statistical uncertainty and (syst) the systematic uncertainty; Extracted neutron $\gamma_0^{n, res}$ (resonance) after applying nuclear corrections to the previous column; Total $\gamma_0^n(Q^2)$; Comparing the two last columns shows that the unmeasured parts of $\gamma_0^n(Q^2)$, i.e, the contributions for $\nu > \nu_{max}$, are negligible.

Q^2 [GeV 2]	ν_{max} (W_{max}) [GeV]	$I_{LT}^{^3He, res}(Q^2) \pm (\text{stat}) \pm (\text{syst})$	$I_{LT}^{n, res}(Q^2) \pm (\text{stat}) \pm (\text{syst})$	$I_{LT}(Q^2)^n \pm (\text{stat}) \pm (\text{syst})$
0.035	1.690 (2.00)	$-0.326 \pm 0.272 \pm 0.520$	$-0.294 \pm 0.316 \pm 0.604$	$-1.112 \pm 0.316 \pm 0.606$
0.057	1.700 (2.00)	$0.285 \pm 0.117 \pm 0.333$	$0.413 \pm 0.136 \pm 0.387$	$-0.862 \pm 0.136 \pm 0.389$
0.079	1.710 (2.00)	$0.610 \pm 0.128 \pm 0.268$	$0.786 \pm 0.149 \pm 0.312$	$-0.721 \pm 0.149 \pm 0.314$
0.100	2.885 (2.49)	$0.879 \pm 0.098 \pm 0.280$	$1.092 \pm 0.114 \pm 0.327$	$-0.126 \pm 0.114 \pm 0.329$
0.150	2.910 (2.48)	$0.339 \pm 0.049 \pm 0.198$	$0.458 \pm 0.057 \pm 0.231$	$-0.266 \pm 0.057 \pm 0.233$
0.200	2.655 (2.38)	$0.289 \pm 0.047 \pm 0.228$	$0.389 \pm 0.055 \pm 0.265$	$-0.345 \pm 0.055 \pm 0.267$
0.240	2.320 (2.23)	$0.391 \pm 0.057 \pm 0.163$	$0.511 \pm 0.067 \pm 0.190$	$-0.267 \pm 0.067 \pm 0.192$

TABLE III: Data and kinematics for $I_{LT}(Q^2)$. From left to right: Four-momentum transfer squared; Maximum ν value experimentally covered (equivalent maximum invariant W ($W = (M^2 + 2M\nu - Q^2)^{1/2}$); $I_{LT}^{^3He, res}(Q^2)$ measured over the ν (W) range from pion threshold up to maximum ν (W) covered experimentally (mostly the nucleon resonance region) and before applying the nuclear corrections to extract the neutron information. (stat) denotes the statistical uncertainty and (syst) the systematic uncertainty; Extracted neutron $I_{LT}^{n, res}$ (resonance) after applying nuclear corrections to the previous column; Total $I_{LT}^n(Q^2)$, including an estimate for the unmeasured contribution above ν_{max} .

Q^2 [GeV 2]	ν [MeV]	W [MeV]	x	σ_{LT} [μ b]	Stat.	Uncor. syst.	Cor. syst.	σ_{TT} [μ b]	Stat.	Uncor. syst.	Cor. syst.
0.035	167.5	1076.9	0.1114	-29.593	7.821	4.430	6.567	-50.779	8.849	4.803	7.200
0.035	210.0	1113.3	0.0888	-9.283	8.641	4.463	2.718	-60.029	9.257	4.828	3.067
0.035	250.0	1146.5	0.0746	5.012	7.507	7.804	4.201	-70.097	7.608	10.592	5.505
0.035	290.0	1178.8	0.0643	-4.189	8.133	4.768	4.598	-144.587	7.398	6.008	5.937
0.035	330.0	1210.2	0.0565	-11.970	7.757	5.264	4.145	-180.197	6.794	8.238	5.752
0.035	370.0	1240.8	0.0504	3.328	7.025	5.624	3.348	-159.284	6.028	7.449	5.188
0.035	410.0	1270.7	0.0455	7.802	6.144	4.136	2.339	-102.038	5.192	5.252	3.146
0.035	450.0	1299.9	0.0414	2.569	6.034	1.754	1.333	-56.856	4.689	3.063	1.734
0.035	490.0	1328.5	0.0381	-2.776	6.006	1.077	1.003	-36.599	4.210	2.488	1.797
0.035	530.0	1356.4	0.0352	-0.849	5.748	0.699	2.120	-22.279	3.827	1.881	2.340
0.035	570.0	1383.8	0.0327	4.796	6.483	0.646	0.845	-17.020	4.317	1.184	2.026
0.035	610.0	1410.7	0.0306	7.627	9.229	0.833	0.899	-19.965	7.244	1.079	2.128
0.035	650.0	1437.0	0.0287	11.711	10.295	0.878	0.757	-13.732	8.808	0.690	1.336
0.035	690.0	1462.9	0.0270	22.036	10.449	1.301	1.731	-18.433	8.192	0.832	1.271
0.035	730.0	1488.4	0.0256	10.433	10.676	1.255	3.585	-17.674	6.646	0.939	1.543
0.035	770.0	1513.4	0.0242	-16.164	9.879	0.690	2.002	-9.317	5.897	0.830	1.388
0.035	810.0	1538.0	0.0230	-3.384	10.144	0.905	2.704	-13.691	5.873	1.137	1.231
0.035	850.0	1562.2	0.0219	6.799	11.135	0.939	3.434	-16.569	6.153	1.448	2.080
0.035	890.0	1586.0	0.0210	-5.700	10.532	0.600	3.009	-9.035	5.791	0.515	2.530
0.035	930.0	1609.5	0.0201	17.363	10.209	0.852	1.794	-18.818	5.628	0.690	1.982
0.035	970.0	1632.7	0.0192	8.494	9.638	0.846	1.477	-21.969	4.806	1.291	0.844
0.035	1010.0	1655.5	0.0185	-8.975	8.213	0.660	1.582	-25.754	4.428	1.639	1.197
0.035	1050.0	1678.0	0.0178	-14.309	7.307	0.924	1.935	-15.582	4.476	1.424	1.432
0.035	1090.0	1700.2	0.0171	3.170	8.109	0.537	2.119	-13.869	4.743	0.862	0.833
0.035	1130.0	1722.2	0.0165	-8.033	9.470	0.818	2.159	-8.614	5.365	0.660	0.765
0.035	1170.0	1743.8	0.0159	-15.669	9.088	0.909	2.006	-14.402	5.160	2.370	1.013

0.035	1210.0	1765.2	0.0154	-3.340	9.120	0.257	0.488	-20.220	5.268	1.405	2.551
0.035	1250.0	1786.3	0.0149	8.626	9.670	0.657	1.584	-17.874	5.217	0.934	1.967
0.035	1290.0	1807.2	0.0145	6.658	9.509	0.504	0.796	-22.003	5.059	1.209	1.012
0.035	1330.0	1827.9	0.0140	10.562	9.728	0.755	1.773	-17.263	5.284	0.894	0.558
0.035	1370.0	1848.3	0.0136	-6.227	10.036	0.190	1.003	-15.983	5.941	0.877	0.438
0.035	1410.0	1868.5	0.0132	-0.496	10.253	0.396	1.494	-17.223	6.110	0.925	0.429
0.035	1450.0	1888.5	0.0129	9.730	10.555	0.963	2.563	-17.723	6.335	0.921	0.561
0.035	1490.0	1908.2	0.0125	-16.688	10.365	0.758	1.789	-15.680	6.315	0.938	0.887
0.035	1530.0	1927.8	0.0122	-6.735	10.420	0.298	0.434	-26.546	6.354	1.474	1.010
0.035	1570.0	1947.2	0.0119	-3.131	11.567	0.146	0.590	-16.390	6.927	0.895	0.547
0.035	1610.0	1966.4	0.0116	-12.388	12.041	0.576	1.025	-15.621	7.166	0.876	0.443
0.035	1650.0	1985.4	0.0113	-25.057	12.833	1.492	2.250	-11.943	7.797	0.939	0.488
0.035	1690.0	2004.2	0.0110	12.734	13.111	0.708	1.519	-16.559	8.754	2.147	0.546
0.035	1730.0	2022.8	0.0108	-3.404	12.912	0.180	0.339	-23.472	8.469	1.405	0.496
0.035	1770.0	2041.3	0.0105	-18.275	10.605	0.945	0.752	-10.813	8.329	0.977	0.719
0.035	1810.0	2059.6	0.0103	-6.756	11.453	0.312	1.048	-23.516	7.914	1.303	1.315
0.035	1850.0	2077.7	0.0101	-18.357	14.142	1.001	0.658	-1.761	10.219	0.197	0.559
0.057	177.5	1075.4	0.1712	7.220	15.736	3.537	8.714	-92.373	19.571	4.724	11.368
0.057	220.0	1111.8	0.1381	8.333	7.607	3.298	3.970	-85.011	9.007	3.795	4.741
0.057	260.0	1145.1	0.1168	4.145	6.307	3.452	5.860	-85.636	6.975	3.884	6.973
0.057	300.0	1177.4	0.1013	-11.320	6.279	4.864	6.505	-136.987	6.600	5.833	7.964
0.057	340.0	1208.9	0.0893	3.996	6.344	5.770	5.386	-179.319	6.447	7.269	6.118
0.057	380.0	1239.5	0.0799	16.750	5.973	6.692	6.489	-159.668	5.916	7.136	6.346
0.057	420.0	1269.5	0.0723	14.794	5.623	4.770	4.507	-104.990	5.277	4.722	3.989
0.057	460.0	1298.7	0.0660	16.454	5.864	2.330	2.421	-64.416	5.024	3.446	3.120
0.057	500.0	1327.3	0.0608	13.597	5.883	1.659	4.063	-36.795	4.674	2.493	2.566

0.057	540.0	1355.2	0.0562	4.128	5.647	0.697	2.973	-15.701	4.370	0.971	2.064
0.057	580.0	1382.7	0.0524	-3.473	5.804	0.581	4.200	-11.937	4.380	0.789	2.328
0.057	620.0	1409.5	0.0490	-3.249	6.656	0.632	1.316	-20.045	4.979	1.075	1.765
0.057	660.0	1435.9	0.0460	2.172	7.360	0.474	2.020	-12.806	5.690	0.642	2.699
0.057	700.0	1461.8	0.0434	13.961	7.318	0.966	1.970	-11.075	5.491	0.483	2.133
0.057	740.0	1487.3	0.0410	14.570	7.427	1.118	2.889	-20.931	5.619	0.900	1.405
0.057	780.0	1512.3	0.0389	3.221	7.617	0.675	2.554	-16.318	5.599	0.791	1.357
0.057	820.0	1536.9	0.0370	5.563	7.585	0.637	1.174	-14.062	5.286	0.659	0.750
0.057	860.0	1561.2	0.0353	0.817	7.583	0.307	0.947	-12.846	5.180	0.696	0.753
0.057	900.0	1585.0	0.0338	4.921	7.582	0.588	1.167	-17.092	5.121	0.806	1.163
0.057	940.0	1608.5	0.0323	16.944	8.508	0.796	1.911	-22.979	5.428	1.003	1.584
0.057	980.0	1631.7	0.0310	11.996	9.503	1.179	2.745	-15.319	5.418	1.004	1.096
0.057	1020.0	1654.5	0.0298	-23.536	9.559	1.079	1.610	-9.656	5.365	1.281	0.666
0.057	1060.0	1677.0	0.0287	-26.072	9.871	1.414	3.111	-5.177	5.518	0.649	0.900
0.057	1100.0	1699.3	0.0276	-0.363	10.045	0.119	1.423	-8.255	5.946	0.430	0.809
0.057	1140.0	1721.2	0.0266	-1.114	10.216	0.145	0.423	-13.182	6.421	0.699	0.462
0.057	1180.0	1742.9	0.0257	0.422	10.433	0.162	0.878	-13.824	6.438	0.720	0.435
0.057	1220.0	1764.3	0.0249	3.185	10.857	0.291	0.661	-13.149	6.460	0.667	0.883
0.057	1260.0	1785.4	0.0241	-0.032	11.082	0.142	0.533	-9.820	6.050	0.562	0.857
0.057	1300.0	1806.3	0.0234	3.530	10.636	0.393	0.546	-19.872	5.708	1.107	1.144
0.057	1340.0	1827.0	0.0227	7.619	10.962	0.596	1.217	-16.451	5.826	0.862	1.034
0.057	1380.0	1847.4	0.0220	-3.622	11.395	0.246	0.806	-15.794	6.415	0.868	1.215
0.057	1420.0	1867.6	0.0214	-0.549	11.656	0.357	1.057	-16.219	6.442	0.876	0.915
0.057	1460.0	1887.6	0.0208	7.762	11.952	0.710	1.369	-16.017	6.482	0.825	0.515
0.057	1500.0	1907.4	0.0203	-10.832	11.640	0.617	0.986	-13.847	6.253	0.836	0.717
0.057	1540.0	1927.0	0.0197	-5.680	11.515	0.254	0.371	-21.179	6.064	1.181	0.650

0.057	1580.0	1946.3	0.0192	-1.858	12.504	0.162	0.468	-14.862	6.311	0.812	0.678
0.057	1620.0	1965.5	0.0188	-5.926	12.726	0.461	0.789	-14.826	6.284	0.829	0.619
0.057	1660.0	1984.5	0.0183	-15.284	13.152	1.151	2.330	-11.164	6.518	0.793	0.594
0.057	1700.0	2003.4	0.0179	5.253	13.024	0.574	1.241	-16.632	6.962	1.697	1.296
0.057	1740.0	2022.0	0.0175	-2.795	12.474	0.177	0.293	-21.069	6.512	1.227	0.648
0.057	1780.0	2040.5	0.0171	-11.946	9.985	0.612	1.899	-11.633	6.119	0.893	0.878
0.057	1820.0	2058.8	0.0167	-4.724	10.712	0.237	0.985	-18.421	5.839	1.025	1.079
0.057	1860.0	2076.9	0.0163	-11.979	13.047	0.712	2.817	-4.903	7.290	0.348	0.752
0.079	187.5	1073.9	0.2246	34.143	18.241	3.088	7.411	-64.904	24.672	5.429	10.679
0.079	230.0	1110.4	0.1830	17.772	12.184	3.035	3.783	-92.997	15.691	4.322	5.277
0.079	270.0	1143.7	0.1559	-2.744	8.866	3.869	4.971	-111.705	10.617	4.587	5.878
0.079	310.0	1176.0	0.1358	-12.400	7.942	5.274	5.393	-154.179	9.071	6.282	6.244
0.079	350.0	1207.5	0.1203	11.408	8.144	6.164	5.841	-177.788	9.089	7.241	6.483
0.079	390.0	1238.2	0.1079	34.764	7.864	6.817	4.885	-157.234	8.585	7.005	4.887
0.079	430.0	1268.2	0.0979	33.358	7.078	4.791	2.725	-105.957	7.208	4.616	2.363
0.079	470.0	1297.4	0.0896	22.314	6.960	2.869	1.047	-66.394	6.410	3.677	1.380
0.079	510.0	1326.0	0.0825	18.464	6.282	1.899	1.063	-36.957	5.451	2.386	1.736
0.079	550.0	1354.0	0.0765	13.599	5.490	1.138	0.957	-17.115	4.625	0.778	1.702
0.079	590.0	1381.5	0.0714	-5.347	6.480	0.826	1.173	-11.003	5.262	0.910	1.139
0.079	630.0	1408.4	0.0668	-9.027	6.974	0.677	2.375	-17.658	5.457	1.287	1.825
0.079	670.0	1434.8	0.0628	-3.163	7.671	0.457	2.089	-15.417	5.870	0.967	2.565
0.079	710.0	1460.7	0.0593	6.803	7.476	0.640	2.526	-7.954	5.633	0.483	2.015
0.079	750.0	1486.2	0.0561	14.630	7.207	1.060	2.058	-18.739	5.307	1.055	1.122
0.079	790.0	1511.2	0.0533	9.856	7.011	0.892	1.908	-16.028	4.978	1.029	1.266
0.079	830.0	1535.9	0.0507	9.177	6.570	0.857	1.488	-13.424	4.470	1.107	0.843
0.079	870.0	1560.1	0.0484	0.695	6.005	0.333	1.137	-9.367	4.057	0.889	0.881

0.079	910.0	1584.0	0.0463	5.882	5.417	0.564	0.961	-12.198	3.555	1.055	0.818
0.079	950.0	1607.5	0.0443	11.564	6.316	4.244	0.788	-13.436	4.176	1.958	1.268
0.079	990.0	1630.7	0.0425	12.303	10.534	1.106	2.812	-12.655	5.667	0.773	1.305
0.079	1030.0	1653.5	0.0409	-21.372	10.231	0.955	2.364	-6.450	5.427	1.054	1.287
0.079	1070.0	1676.1	0.0393	-26.240	10.201	1.367	3.819	-3.708	5.380	0.610	1.147
0.079	1110.0	1698.3	0.0379	-2.104	10.257	0.121	1.186	-7.792	5.619	0.419	1.100
0.079	1150.0	1720.3	0.0366	0.965	10.455	0.200	2.524	-14.070	5.978	0.712	1.339
0.079	1190.0	1742.0	0.0354	2.804	10.560	0.224	3.987	-14.248	5.945	0.702	1.186
0.079	1230.0	1763.4	0.0342	5.423	10.901	0.392	1.310	-13.352	5.970	0.643	2.508
0.079	1270.0	1784.5	0.0331	2.133	11.226	0.318	1.516	-10.841	5.678	0.639	0.856
0.079	1310.0	1805.4	0.0321	1.789	9.723	0.412	0.904	-23.168	4.838	1.335	2.538
0.079	1350.0	1826.1	0.0312	5.894	9.835	0.557	1.305	-19.972	4.818	1.087	2.263
0.079	1390.0	1846.5	0.0303	0.030	10.081	0.415	1.938	-19.555	5.131	1.049	2.583
0.079	1430.0	1866.8	0.0294	1.654	10.405	0.479	1.437	-19.315	5.292	1.035	1.709
0.079	1470.0	1886.8	0.0286	6.673	10.523	0.579	1.348	-16.243	5.254	0.834	0.761
0.079	1510.0	1906.5	0.0279	-4.686	10.171	0.596	1.309	-13.888	5.054	0.809	0.828
0.079	1550.0	1926.1	0.0272	-4.896	9.978	0.225	0.786	-17.706	4.908	0.988	0.511
0.079	1590.0	1945.5	0.0265	-0.354	10.333	0.202	0.455	-14.538	4.777	0.786	0.801
0.079	1630.0	1964.7	0.0258	-0.897	10.428	0.442	1.642	-15.400	4.767	0.838	0.931
0.079	1670.0	1983.7	0.0252	-6.199	10.704	0.993	2.901	-11.479	4.933	0.721	0.804
0.079	1710.0	2002.6	0.0246	-1.247	10.500	0.496	1.681	-16.864	5.130	1.390	1.502
0.079	1750.0	2021.2	0.0241	-2.692	9.746	0.187	0.367	-19.326	4.745	1.113	0.728
0.079	1790.0	2039.7	0.0235	-6.890	8.195	0.376	1.963	-13.116	4.471	0.863	0.913
0.079	1830.0	2058.0	0.0230	-3.057	9.057	0.200	0.908	-14.979	4.587	0.833	0.936
0.079	1870.0	2076.2	0.0225	-7.990	10.082	0.521	2.570	-7.945	5.094	0.497	0.747
0.100	202.5	1077.2	0.2632	15.456	8.022	3.954	3.871	-76.998	11.594	6.669	7.076

0.100	245.0	1113.6	0.2175	19.384	7.195	4.030	3.331	-65.123	9.686	5.755	5.130
0.100	285.0	1146.8	0.1870	26.126	5.169	3.594	3.967	-101.549	6.431	4.671	5.009
0.100	325.0	1179.1	0.1640	9.181	5.267	5.300	4.472	-145.831	6.295	6.330	5.300
0.100	365.0	1210.5	0.1460	15.938	5.842	8.753	4.948	-185.663	6.703	9.835	5.651
0.100	405.0	1241.1	0.1316	9.510	5.673	5.847	4.029	-138.361	6.112	6.834	4.482
0.100	445.0	1271.0	0.1198	21.309	5.085	3.680	1.449	-84.572	5.254	4.195	1.821
0.100	485.0	1300.2	0.1099	21.822	4.835	2.374	1.142	-45.411	4.819	2.345	1.578
0.100	525.0	1328.7	0.1015	5.873	5.348	0.828	3.050	-17.056	5.058	0.906	2.513
0.100	565.0	1356.7	0.0943	11.819	4.088	1.243	2.111	-17.313	3.736	1.101	1.720
0.100	605.0	1384.1	0.0881	10.628	3.602	1.331	2.131	-20.914	3.192	1.446	1.485
0.100	645.0	1410.9	0.0826	6.652	4.049	1.041	1.367	-22.418	3.365	1.561	1.095
0.100	685.0	1437.3	0.0778	10.810	4.650	1.263	0.900	-21.760	3.758	1.737	1.250
0.100	725.0	1463.2	0.0735	7.994	4.797	0.884	0.550	-14.369	3.857	1.624	0.831
0.100	765.0	1488.6	0.0697	4.631	4.649	0.766	0.824	-13.315	3.650	1.297	0.902
0.100	805.0	1513.6	0.0662	8.032	4.672	1.190	0.631	-12.766	3.494	1.563	0.877
0.100	845.0	1538.2	0.0631	6.553	4.473	1.124	0.330	-11.851	3.606	1.709	0.640
0.100	885.0	1562.4	0.0602	4.063	4.603	0.570	0.354	-7.306	3.889	1.272	0.615
0.100	925.0	1586.2	0.0576	3.901	4.887	0.682	0.339	-7.039	3.701	1.351	0.521
0.100	965.0	1609.7	0.0552	7.498	10.407	9.152	0.687	-3.231	7.243	3.668	0.847
0.100	1005.0	1632.9	0.0530	8.199	6.938	0.583	0.580	-8.522	4.879	0.443	0.958
0.100	1045.0	1655.7	0.0510	3.330	6.326	1.012	2.855	-19.256	4.404	2.984	1.133
0.100	1085.0	1678.2	0.0491	-5.996	6.643	1.041	3.084	-13.311	4.487	1.578	1.626
0.100	1125.0	1700.4	0.0474	5.958	5.880	0.558	0.716	-14.852	3.817	0.716	0.856
0.100	1165.0	1722.4	0.0457	5.983	6.420	0.522	3.161	-21.348	3.982	1.217	1.772
0.100	1205.0	1744.0	0.0442	-1.774	6.282	0.583	2.308	-19.196	3.834	2.291	1.536
0.100	1245.0	1765.4	0.0428	0.367	6.886	0.344	0.767	-16.672	4.099	1.209	2.685

0.100	1285.0	1786.5	0.0415	8.289	6.606	0.901	2.520	-28.115	3.851	1.665	1.862
0.100	1325.0	1807.4	0.0402	-2.222	9.184	0.268	3.484	-10.811	4.707	0.642	1.507
0.100	1365.0	1828.1	0.0390	1.185	9.278	0.396	1.450	-9.927	4.728	0.561	0.632
0.100	1405.0	1848.5	0.0379	-3.194	9.330	0.228	0.502	-12.630	4.945	0.778	0.957
0.100	1445.0	1868.7	0.0369	-3.062	9.625	0.281	1.343	-4.770	4.941	0.309	3.315
0.100	1485.0	1888.7	0.0359	1.817	9.708	0.369	1.398	-10.809	4.950	0.625	0.566
0.100	1525.0	1908.4	0.0349	-14.830	9.162	0.684	2.861	-19.837	4.816	1.353	3.762
0.100	1565.0	1928.0	0.0341	-2.055	9.173	0.206	0.802	-12.951	4.850	0.779	0.856
0.100	1605.0	1947.4	0.0332	-4.243	9.530	0.193	1.135	-9.340	4.905	0.600	0.611
0.100	1645.0	1966.5	0.0324	2.988	9.658	0.687	1.475	-17.478	5.030	1.073	1.227
0.100	1685.0	1985.5	0.0316	0.209	7.303	0.857	1.807	-12.793	3.697	0.748	0.948
0.100	1725.0	2004.3	0.0309	-6.303	7.199	0.399	1.489	-17.072	3.758	1.158	0.984
0.100	1765.0	2023.0	0.0302	-2.988	7.012	0.190	0.278	-17.894	3.704	1.000	0.489
0.100	1805.0	2041.5	0.0295	-2.567	6.152	0.222	0.989	-14.275	3.386	0.827	0.351
0.100	1845.0	2059.8	0.0289	-2.509	7.388	0.206	0.900	-12.301	3.916	0.688	0.376
0.100	1885.0	2077.9	0.0283	-4.084	7.543	0.436	1.750	-9.504	3.958	0.560	0.562
0.100	2005.0	2131.4	0.0266	3.842	4.597	0.274	0.536	-12.950	2.610	0.675	0.322
0.100	2045.0	2148.9	0.0261	3.536	4.544	0.289	0.070	-12.664	2.563	0.671	0.119
0.100	2085.0	2166.3	0.0256	3.312	4.672	0.275	0.081	-12.602	2.601	0.669	0.123
0.100	2125.0	2183.6	0.0251	3.729	4.758	0.291	0.203	-12.564	2.613	0.666	0.132
0.100	2165.0	2200.7	0.0246	3.467	6.179	0.425	1.015	-12.002	3.365	0.643	0.216
0.100	2205.0	2217.7	0.0242	-7.082	9.019	0.380	0.589	-11.031	4.931	0.664	0.175
0.100	2245.0	2234.6	0.0237	3.104	7.672	0.268	0.255	-15.142	4.189	0.852	0.169
0.100	2285.0	2251.3	0.0233	1.188	7.367	0.201	0.225	-14.907	4.014	0.850	0.208
0.100	2325.0	2267.9	0.0229	0.464	4.258	0.150	0.231	-12.881	2.418	0.662	0.364
0.100	2365.0	2284.4	0.0225	3.874	4.411	0.287	0.739	-10.969	2.221	0.630	0.435

0.100	2405.0	2300.8	0.0222	-3.542	4.432	0.404	1.238	-11.716	2.166	0.681	0.430
0.100	2445.0	2317.0	0.0218	-2.553	4.665	0.329	1.321	-10.259	2.300	0.588	0.452
0.100	2485.0	2333.2	0.0214	-0.625	5.832	0.631	1.708	-8.202	3.259	0.638	0.364
0.100	2525.0	2349.2	0.0211	-4.785	5.523	0.537	1.282	-12.208	3.150	0.733	0.456
0.100	2565.0	2365.1	0.0208	-5.088	5.431	0.310	1.000	-8.565	2.863	0.495	0.953
0.100	2605.0	2380.9	0.0205	-4.249	6.307	0.211	0.465	-7.268	3.132	0.448	1.061
0.100	2645.0	2396.6	0.0201	-1.454	6.765	0.106	0.354	-12.333	3.318	0.730	0.448
0.100	2685.0	2412.2	0.0198	-3.477	7.573	0.214	0.650	-13.003	3.659	0.759	0.300
0.100	2725.0	2427.7	0.0196	-8.275	8.178	0.403	0.726	-13.838	4.016	0.831	0.316
0.100	2765.0	2443.2	0.0193	-5.867	7.309	0.298	0.926	-15.363	4.422	0.968	1.116
0.100	2805.0	2458.5	0.0190	-2.355	7.693	0.229	0.668	-15.399	5.141	1.072	1.665
0.100	2845.0	2473.7	0.0187	-5.013	6.881	0.306	0.212	-12.836	4.092	0.743	0.682
0.100	2885.0	2488.8	0.0185	-4.007	7.609	0.178	1.216	-15.019	4.365	0.880	1.561
0.150	227.5	1075.8	0.3514	3.537	6.103	9.555	8.491	-61.256	10.170	11.998	11.833
0.150	270.0	1112.2	0.2961	12.933	5.666	2.324	5.877	-50.296	8.559	3.450	9.452
0.150	310.0	1145.5	0.2579	25.440	4.679	2.025	7.919	-94.374	6.515	3.322	9.936
0.150	350.0	1177.8	0.2284	10.614	4.508	3.682	6.815	-143.747	5.921	4.929	8.771
0.150	390.0	1209.2	0.2050	4.516	4.762	5.869	6.254	-172.890	5.986	7.373	7.870
0.150	430.0	1239.9	0.1859	5.435	5.039	4.319	4.480	-131.759	6.205	5.353	5.498
0.150	470.0	1269.8	0.1701	9.906	4.742	3.185	1.466	-84.240	5.769	4.149	1.659
0.150	510.0	1299.0	0.1567	8.116	4.447	2.427	0.564	-49.114	5.182	3.235	0.789
0.150	550.0	1327.6	0.1453	7.676	3.913	1.581	0.962	-28.701	4.284	2.042	1.501
0.150	590.0	1355.5	0.1355	8.485	3.482	1.581	0.894	-20.635	3.634	1.832	1.424
0.150	630.0	1383.0	0.1269	8.687	3.196	1.663	0.799	-18.807	3.235	2.089	1.208
0.150	670.0	1409.8	0.1193	8.416	3.141	1.160	1.107	-16.606	3.148	1.882	1.194
0.150	710.0	1436.2	0.1126	6.033	3.297	0.852	0.856	-14.093	3.397	1.168	1.285

0.150	750.0	1462.1	0.1066	7.997	3.653	0.433	0.693	-10.516	3.717	0.663	1.011
0.150	790.0	1487.6	0.1012	9.738	4.130	0.866	1.523	-8.556	3.763	1.072	1.499
0.150	830.0	1512.6	0.0963	2.912	4.650	1.160	2.293	-3.873	3.830	0.970	2.076
0.150	870.0	1537.2	0.0919	3.913	4.955	1.031	1.372	-5.819	4.151	1.259	1.293
0.150	910.0	1561.4	0.0878	1.937	5.032	0.322	1.756	-2.842	4.165	0.739	2.246
0.150	950.0	1585.3	0.0841	0.456	4.813	0.523	2.733	-6.978	3.791	0.905	1.895
0.150	990.0	1608.8	0.0807	14.691	8.089	1.680	1.313	-16.938	5.876	1.031	1.181
0.150	1030.0	1631.9	0.0776	3.467	4.850	0.282	1.390	-6.773	3.744	0.312	0.817
0.150	1070.0	1654.8	0.0747	1.026	4.520	0.336	3.396	-12.652	3.690	0.675	1.371
0.150	1110.0	1677.3	0.0720	-9.527	4.579	0.439	0.637	-8.883	3.715	0.701	0.726
0.150	1150.0	1699.5	0.0695	-2.496	4.546	0.339	1.135	-10.505	3.456	0.620	0.495
0.150	1190.0	1721.5	0.0672	2.371	4.692	0.317	2.825	-13.350	3.472	0.673	1.156
0.150	1230.0	1743.1	0.0650	-1.243	4.488	0.380	1.791	-13.722	3.419	1.102	0.724
0.150	1270.0	1764.5	0.0629	6.832	5.027	0.665	1.436	-16.786	3.863	0.914	1.377
0.150	1310.0	1785.7	0.0610	10.278	6.246	1.002	1.441	-17.229	4.181	0.953	0.635
0.150	1350.0	1806.6	0.0592	-5.703	6.405	0.230	1.623	-6.508	4.207	0.473	0.739
0.150	1390.0	1827.2	0.0575	-3.262	6.414	0.275	0.385	-6.172	4.219	0.424	0.589
0.150	1430.0	1847.7	0.0559	-1.099	6.157	0.284	0.697	-12.787	4.285	0.806	0.952
0.150	1470.0	1867.8	0.0544	-4.573	7.312	0.282	0.403	-0.691	4.506	0.127	0.559
0.150	1510.0	1887.8	0.0529	-1.400	7.457	0.157	0.385	-7.804	4.531	0.507	0.342
0.150	1550.0	1907.6	0.0516	-13.139	6.321	0.736	0.198	-20.054	4.098	1.409	0.202
0.150	1590.0	1927.2	0.0503	2.114	6.761	0.262	0.327	-9.427	4.236	0.565	0.139
0.150	1630.0	1946.6	0.0490	-2.797	6.089	0.247	0.319	-7.940	3.750	0.528	0.207
0.150	1670.0	1965.8	0.0479	9.262	6.393	0.764	0.528	-17.845	3.881	1.020	0.214
0.150	1710.0	1984.8	0.0467	3.543	4.445	0.773	2.983	-12.193	2.476	0.661	0.843
0.150	1750.0	2003.6	0.0457	-10.549	4.368	0.358	1.964	-12.722	2.418	0.789	0.593

0.150	1790.0	2022.2	0.0447	-1.536	4.307	0.243	0.227	-14.143	2.386	0.781	0.312
0.150	1830.0	2040.7	0.0437	3.487	3.931	0.384	0.864	-14.068	2.187	0.743	0.288
0.150	1870.0	2059.0	0.0427	1.752	4.319	0.330	0.782	-13.281	2.276	0.725	0.529
0.150	1910.0	2077.2	0.0419	-1.936	4.157	0.259	1.197	-11.872	2.187	0.679	0.343
0.150	1950.0	2095.1	0.0410	3.002	4.098	0.427	1.225	-10.719	2.254	0.594	0.517
0.150	1990.0	2113.0	0.0402	-5.769	4.182	0.278	0.932	-8.489	2.467	0.518	0.451
0.150	2030.0	2130.7	0.0394	0.327	4.132	0.156	0.364	-12.323	3.232	0.679	0.221
0.150	2070.0	2148.2	0.0386	-0.294	4.412	0.145	0.286	-12.112	3.424	0.675	0.137
0.150	2110.0	2165.6	0.0379	-0.836	4.747	0.136	0.261	-12.090	3.619	0.679	0.139
0.150	2150.0	2182.9	0.0372	-1.796	6.129	0.163	0.305	-11.343	3.367	0.646	0.148
0.150	2190.0	2200.0	0.0365	7.273	6.624	0.496	0.202	-11.858	3.544	0.630	0.145
0.150	2230.0	2217.0	0.0358	0.350	6.497	0.130	0.355	-10.022	3.422	0.565	0.160
0.150	2270.0	2233.9	0.0352	-2.228	5.215	0.119	0.253	-11.921	3.702	0.679	0.179
0.150	2310.0	2250.6	0.0346	-1.973	5.038	0.124	0.367	-12.010	3.503	0.729	0.237
0.150	2350.0	2267.2	0.0340	-2.392	4.845	0.146	0.486	-11.864	3.313	0.873	0.550
0.150	2390.0	2283.7	0.0334	6.938	5.780	0.460	1.499	-9.429	2.599	0.548	0.737
0.150	2430.0	2300.1	0.0329	-7.159	5.875	0.716	2.450	-9.369	2.500	0.612	0.803
0.150	2470.0	2316.3	0.0324	-7.662	5.669	0.419	2.665	-8.457	2.455	0.526	0.718
0.150	2510.0	2332.5	0.0318	-11.704	5.834	0.413	3.805	-6.864	2.889	0.452	0.703
0.150	2550.0	2348.5	0.0313	-12.251	5.803	0.497	3.442	-8.156	2.970	0.566	0.695
0.150	2590.0	2364.4	0.0309	-2.773	6.027	0.516	2.832	-5.731	2.812	0.359	1.226
0.150	2630.0	2380.3	0.0304	-1.879	6.743	0.276	1.265	-6.109	3.010	0.386	1.347
0.150	2670.0	2396.0	0.0299	0.356	6.534	0.110	0.490	-11.304	2.891	0.655	0.434
0.150	2710.0	2411.6	0.0295	-0.429	6.377	0.185	0.460	-11.109	2.753	0.643	0.483
0.150	2750.0	2427.1	0.0291	-4.804	7.336	0.277	4.534	-9.701	2.939	0.590	0.729
0.150	2790.0	2442.5	0.0287	0.726	6.995	0.418	2.757	-12.856	3.135	0.705	2.397

0.150	2830.0	2457.8	0.0282	6.860	6.432	0.509	0.653	-13.259	3.183	0.774	2.246
0.150	2870.0	2473.1	0.0279	1.415	5.449	0.366	0.752	-10.079	2.562	0.629	0.588
0.150	2910.0	2488.2	0.0275	-3.242	5.784	0.087	1.329	-7.754	2.637	0.496	0.747
0.200	252.5	1074.3	0.4221	13.790	3.318	10.709	7.560	-38.694	6.467	14.450	11.419
0.200	295.0	1110.8	0.3613	9.440	3.819	1.772	3.899	-67.255	6.461	2.727	7.448
0.200	335.0	1144.1	0.3181	6.040	3.367	1.457	4.517	-93.382	5.187	2.519	7.215
0.200	375.0	1176.5	0.2842	2.222	3.248	2.957	5.386	-135.555	4.669	4.306	7.699
0.200	415.0	1207.9	0.2568	1.626	3.529	3.853	5.221	-150.585	4.786	5.154	6.992
0.200	455.0	1238.6	0.2342	6.285	3.749	3.791	3.749	-132.563	4.892	4.953	4.900
0.200	495.0	1268.6	0.2153	12.098	3.308	2.779	1.806	-83.584	4.189	3.587	2.171
0.200	535.0	1297.8	0.1992	7.023	4.035	1.809	1.064	-48.229	4.965	2.323	1.226
0.200	575.0	1326.4	0.1854	6.935	5.100	1.208	0.692	-30.576	6.097	1.489	0.859
0.200	615.0	1354.4	0.1733	7.341	4.967	1.082	0.486	-24.222	5.800	1.276	0.729
0.200	655.0	1381.8	0.1627	4.639	4.694	0.865	1.129	-18.166	5.372	1.073	1.064
0.200	695.0	1408.7	0.1534	3.931	4.665	0.465	1.293	-9.967	5.240	0.648	1.100
0.200	735.0	1435.1	0.1450	3.131	4.572	0.514	0.634	-13.385	5.003	0.670	0.769
0.200	775.0	1461.0	0.1375	8.223	4.833	0.548	0.294	-11.448	4.895	0.505	0.480
0.200	815.0	1486.5	0.1308	5.739	4.748	0.399	0.370	-6.351	4.691	0.421	0.376
0.200	855.0	1511.6	0.1247	-6.748	4.703	0.476	0.971	0.020	4.560	0.362	0.646
0.200	895.0	1536.2	0.1191	-2.512	4.395	0.310	1.484	-2.180	4.243	0.223	0.887
0.200	935.0	1560.4	0.1140	1.714	3.861	0.168	0.450	-5.796	3.710	0.240	0.312
0.200	975.0	1584.3	0.1093	-2.916	3.869	0.225	0.645	-3.320	3.575	0.233	0.430
0.200	1015.0	1607.8	0.1050	0.873	3.603	0.197	0.730	-2.289	3.234	0.138	0.436
0.200	1055.0	1631.0	0.1010	3.411	3.369	0.260	0.408	-6.416	2.977	0.303	0.442
0.200	1095.0	1653.8	0.0973	0.917	3.160	0.313	0.612	-8.377	2.874	0.424	0.417
0.200	1135.0	1676.4	0.0939	-5.114	3.164	0.227	0.571	-6.155	2.851	0.423	0.278

0.200	1175.0	1698.6	0.0907	-1.376	3.306	0.289	0.562	-8.777	2.679	0.469	0.309
0.200	1215.0	1720.6	0.0877	-0.408	3.322	0.192	0.583	-7.995	2.632	0.402	0.504
0.200	1255.0	1742.2	0.0849	-2.934	3.316	0.269	0.652	-10.711	2.603	0.594	0.281
0.200	1295.0	1763.7	0.0823	6.539	3.535	0.628	0.385	-15.119	2.762	0.751	0.232
0.200	1335.0	1784.8	0.0798	4.969	4.095	0.587	0.663	-14.784	2.905	0.781	0.283
0.200	1375.0	1805.7	0.0775	8.241	4.053	0.696	0.874	-17.368	3.007	0.870	1.131
0.200	1415.0	1826.4	0.0753	0.926	3.820	0.250	0.803	-10.907	2.816	0.584	1.000
0.200	1455.0	1846.8	0.0733	3.559	3.600	0.372	0.670	-12.090	2.645	0.596	0.728
0.200	1495.0	1867.0	0.0713	0.530	3.654	0.316	0.729	-15.627	2.638	0.827	0.344
0.200	1535.0	1887.0	0.0694	-4.291	3.955	0.254	0.595	-10.485	2.692	0.618	0.387
0.200	1575.0	1906.8	0.0677	3.464	4.031	0.439	0.637	-10.308	2.640	0.540	0.265
0.200	1615.0	1926.4	0.0660	8.330	3.991	0.567	0.499	-10.810	2.576	0.524	0.186
0.200	1655.0	1945.8	0.0644	3.729	4.024	0.344	0.748	-10.536	2.561	0.545	0.262
0.200	1695.0	1965.0	0.0629	6.435	4.111	0.493	1.400	-12.606	2.557	0.635	0.403
0.200	1735.0	1984.0	0.0614	-0.882	4.177	0.696	2.282	-9.990	2.533	0.611	0.659
0.200	1775.0	2002.8	0.0600	-8.126	4.105	0.369	1.713	-8.385	2.429	0.567	0.547
0.200	1815.0	2021.5	0.0587	0.684	4.115	0.317	0.175	-11.252	2.415	0.613	0.357
0.200	1855.0	2039.9	0.0575	4.958	4.019	0.557	0.802	-12.005	2.325	0.633	0.385
0.200	1895.0	2058.2	0.0562	3.502	3.838	0.377	1.037	-13.349	2.130	0.708	0.566
0.200	1935.0	2076.4	0.0551	0.067	3.829	0.229	0.877	-11.955	2.073	0.659	0.348
0.200	1975.0	2094.4	0.0540	1.574	3.852	0.309	0.829	-12.275	2.045	0.673	0.556
0.200	2015.0	2112.2	0.0529	-3.076	3.872	0.163	0.606	-9.834	2.166	0.562	0.458
0.200	2055.0	2129.9	0.0519	-0.166	3.756	0.144	0.447	-10.504	2.661	0.580	0.251
0.200	2095.0	2147.5	0.0509	0.521	3.764	0.190	0.628	-12.039	2.622	0.655	0.304
0.200	2135.0	2164.9	0.0499	-0.129	3.769	0.174	0.766	-12.558	2.555	0.687	0.374
0.200	2175.0	2182.2	0.0490	-2.033	4.404	0.130	0.701	-10.399	2.292	0.585	0.248

0.200	2215.0	2199.3	0.0481	3.207	4.469	0.320	0.843	-10.564	2.364	0.558	0.220
0.200	2255.0	2216.3	0.0473	-1.724	4.238	0.166	1.127	-8.273	2.255	0.465	0.276
0.200	2295.0	2233.2	0.0464	-4.587	3.704	0.186	0.530	-8.809	2.296	0.508	0.191
0.200	2335.0	2249.9	0.0456	-0.694	3.681	0.140	0.571	-8.788	2.071	0.722	0.258
0.200	2375.0	2266.5	0.0449	-1.545	4.021	0.248	0.394	-7.649	2.309	1.340	0.537
0.200	2415.0	2283.0	0.0441	1.542	4.321	0.191	0.822	-10.287	2.297	0.533	0.464
0.200	2455.0	2299.4	0.0434	0.391	5.027	0.110	0.113	-8.194	2.753	0.445	0.151
0.200	2495.0	2315.7	0.0427	3.748	4.711	0.295	0.214	-9.663	2.251	0.516	0.150
0.200	2535.0	2331.8	0.0420	-3.462	5.315	0.176	0.098	-8.667	2.675	0.512	0.156
0.200	2575.0	2347.9	0.0414	-4.257	5.050	0.185	0.200	-8.722	2.502	0.549	0.173
0.200	2615.0	2363.8	0.0408	8.723	4.601	0.583	0.728	-8.317	2.103	0.429	0.275
0.200	2655.0	2379.6	0.0401	3.937	5.560	0.269	0.943	-9.021	2.691	0.494	0.336
0.240	277.5	1077.6	0.4609	14.650	4.723	4.956	2.176	-58.830	9.270	11.761	6.767
0.240	320.0	1113.9	0.3997	12.332	5.068	3.379	2.528	-70.081	8.721	6.884	5.335
0.240	360.0	1147.1	0.3553	7.192	3.694	2.159	2.890	-88.335	5.967	3.823	4.975
0.240	400.0	1179.4	0.3197	2.021	3.783	3.169	3.019	-120.832	5.717	4.758	4.737
0.240	440.0	1210.8	0.2907	4.501	3.909	3.769	3.340	-137.414	5.594	5.342	4.805
0.240	480.0	1241.4	0.2664	6.774	3.906	3.661	3.144	-128.423	5.340	4.992	4.292
0.240	520.0	1271.3	0.2460	14.674	3.778	2.474	1.586	-80.133	4.966	3.240	2.040
0.240	560.0	1300.5	0.2284	7.420	4.538	1.556	0.935	-49.234	5.786	1.970	1.101
0.240	600.0	1329.0	0.2132	7.277	5.292	1.062	0.343	-31.454	6.538	1.279	0.407
0.240	640.0	1357.0	0.1998	7.134	4.791	0.877	0.302	-25.574	5.755	1.026	0.413
0.240	680.0	1384.3	0.1881	5.395	4.392	0.649	0.732	-19.033	5.145	0.738	0.730
0.240	720.0	1411.2	0.1776	5.324	4.210	0.398	0.796	-8.635	4.816	0.359	0.743
0.240	760.0	1437.5	0.1683	5.075	3.738	0.433	0.466	-9.629	4.143	0.443	0.651
0.240	800.0	1463.4	0.1599	11.109	3.709	0.816	0.378	-9.196	3.833	0.620	0.465

0.240	840.0	1488.8	0.1523	8.491	3.343	0.508	0.572	-3.113	3.381	0.434	0.539
0.240	880.0	1513.8	0.1453	-1.176	3.047	0.373	1.171	-0.789	3.030	0.312	0.940
0.240	920.0	1538.4	0.1390	0.851	2.695	0.282	0.745	-6.161	2.672	0.281	0.580
0.240	960.0	1562.6	0.1332	0.765	2.565	0.229	0.344	-7.973	2.506	0.365	0.296
0.240	1000.0	1586.5	0.1279	2.504	2.841	0.333	0.620	-4.932	2.610	0.266	0.657
0.240	1040.0	1610.0	0.1230	7.956	3.699	0.488	0.925	-5.591	3.240	0.376	0.993
0.240	1080.0	1633.1	0.1184	8.457	3.690	0.610	1.337	-10.510	3.174	0.581	0.804
0.240	1120.0	1655.9	0.1142	7.155	3.552	0.714	1.814	-8.929	2.983	0.686	0.918
0.240	1160.0	1678.4	0.1103	-2.486	3.677	0.271	1.572	-4.796	3.045	0.353	0.780
0.240	1200.0	1700.7	0.1066	3.012	4.048	0.286	0.734	-8.299	3.277	0.380	0.531
0.240	1240.0	1722.6	0.1031	-0.472	4.318	0.124	0.329	-4.527	3.370	0.244	0.461
0.240	1280.0	1744.2	0.0999	-2.042	4.252	0.242	0.593	-8.851	3.259	0.499	0.351
0.240	1320.0	1765.6	0.0969	5.330	4.242	0.478	0.522	-11.534	3.199	0.539	0.244
0.240	1360.0	1786.7	0.0940	1.181	4.249	0.345	0.447	-12.226	3.152	0.633	0.312
0.240	1400.0	1807.6	0.0914	10.185	4.394	0.741	1.519	-13.575	3.332	0.628	0.599
0.240	1440.0	1828.3	0.0888	1.459	4.292	0.188	0.128	-7.033	3.187	0.365	0.150
0.240	1480.0	1848.7	0.0864	2.829	4.054	0.323	0.300	-8.625	2.967	0.439	0.308
0.240	1520.0	1868.9	0.0841	-1.767	3.848	0.250	0.831	-13.948	2.755	0.781	1.197
0.240	1560.0	1888.8	0.0820	-4.030	4.057	0.270	0.714	-9.832	2.685	0.603	0.357
0.240	1600.0	1908.6	0.0799	5.364	3.852	0.389	1.677	-9.721	2.455	0.478	1.420
0.240	1640.0	1928.2	0.0780	6.050	3.600	0.506	1.492	-10.500	2.293	0.543	0.503
0.240	1680.0	1947.5	0.0761	3.945	3.470	0.354	0.943	-10.827	2.190	0.613	0.329
0.240	1720.0	1966.7	0.0744	3.671	3.498	0.356	1.263	-10.053	2.174	0.515	0.443
0.240	1760.0	1985.7	0.0727	-0.841	3.164	0.523	1.685	-8.908	1.963	0.560	0.538
0.240	1800.0	2004.5	0.0711	-2.307	3.086	0.324	1.077	-8.801	1.749	0.512	0.415
0.240	1840.0	2023.2	0.0695	3.159	3.330	0.376	0.155	-10.280	2.061	0.531	0.255

0.240	1880.0	2041.6	0.0680	2.450	3.275	0.338	0.899	-10.236	2.031	0.549	0.319
0.240	1920.0	2059.9	0.0666	0.830	3.171	0.200	0.731	-9.732	1.944	0.521	0.482
0.240	1960.0	2078.1	0.0653	3.365	3.127	0.333	0.535	-11.821	1.916	0.607	0.291
0.240	2000.0	2096.1	0.0639	0.102	2.949	0.204	0.575	-11.153	1.617	0.600	0.391
0.240	2040.0	2113.9	0.0627	-1.216	2.907	0.134	0.449	-9.477	1.765	0.520	0.254
0.240	2080.0	2131.6	0.0615	1.361	3.078	0.192	0.110	-8.447	1.934	0.440	0.203
0.240	2120.0	2149.1	0.0603	3.651	3.059	0.350	0.350	-13.124	1.902	0.668	0.527
0.240	2160.0	2166.5	0.0592	1.622	3.051	0.244	0.600	-12.831	1.743	0.668	0.624
0.240	2200.0	2183.8	0.0581	-0.408	3.305	0.128	0.444	-10.021	1.960	0.535	0.308
0.240	2240.0	2200.9	0.0571	-1.516	3.507	0.153	0.317	-8.893	2.203	0.486	0.206
0.240	2280.0	2217.8	0.0561	-5.569	3.579	0.245	0.334	-6.705	2.221	0.405	0.214
0.240	2320.0	2234.7	0.0551	-4.849	3.695	0.278	0.720	-7.365	2.189	0.426	0.198

TABLE IV: Table of $\sigma_{\text{LT}}(\nu, Q^2)$ and $\sigma_{\text{TT}}(\nu, Q^2)$ on ${}^3\text{He}$. From left to right: Four-momentum transfer squared; energy transfer ν ; Invariant mass W ; Bjorken scaling variable x ; Cross-section, statistical uncertainty, uncorrelated systematic uncertainty, and correlated uncertainty for σ_{LT} and σ_{TT} , respectively.